J Mater Sci (2007) 42:6439–6445
DOI 10.1007/s10853-006-1202-5

Preparation and characterization of SiC nanowires and nanoparticles from filter paper by sol–gel and carbothermal reduction processing

Wei Wang · ZhiHao Jin · Tao Xue · GangBin Yang · GuanJun Qiao

Received: 28 February 2006 / Accepted: 31 October 2006 / Published online: 25 April 2007

Abstract The carbothermal reduction of SiO_2 gel containing filter paper (as carbon precursors) in argon was used to prepare SiC nanowires and nanoparticles. The resulting SiC ceramic, as well as the conversion mechanism of carbon/silica composites to SiC nanowires and nanoparticles, have been investigated by scanning electron microscopy (SEM), Transmission electron microscopy (TEM), x-ray diffraction (XRD), Fourier transform infrared spectroscopy (FTIR), and thermogravimetric analysis (TG) techniques. XRD and IR studies show that the materials, obtained from reaction at 1550 °C for 1 h in static argon atmosphere, are β-SiC. SEM and TEM reveal that SiC nanowires is single crystal wires with diameters ranging from 50–200 nm and their lengths over several tens of microns. According to thermodynamic analysis, SiC nanowires and SiC nanoparticles in the resulting SiC ceramic are formed by gas-gas reaction of SiO (g) and CO (g).

Introduction

Various types of nanomaterials (nanowires, nanotubes, or nanorods) have become the focus of intensive research for their potential applications in nanoscience and nanotechnology [1–4]. Among these nanomaterials, silicon carbide (SiC) nanowires are effective materials for the reinforcement of various composite materials because of their high strength and stiffness combined with large aspect ratios. The strengths of the SiC nanorods measured were substantially greater than those found previously for larger SiC structures, and they approach theoretical values [4]. Several techniques have been applied to synthesize SiC nanowires, including physical evaporation [5], chemical vapor deposition [6–9], laser ablation [10–12] and carbothermal reduction of silica [13, 14]. The last method is preferred for mass production because of its inherent advantages, the low-cost raw materials (SiO_2 and carbon) and the simplicity of the production procedures.

There have been a lot of researches in the carbothermal reduction of silica for preparing SiC nanomaterials. Won-Seon Seo used carbon black powder and silica powder to synthesize β-silicon carbon whisker [15]. The carbothermal reduction of SiO_2 xerogel by carbon nanoparticles was used to prepare different kind of SiC nanostructures [16, 17]. However, previous works focused on utilizing carbon as the starting materials, few studies have reported on converting the carbon precursors (paper, et al.) into ceramic materials [18, 19]. Up till now, there is no report about the preparation of SiC nanowires and nanoparticles from filter paper by sol–gel and carbothermal reduction processing.

This report describes the use of filter paper (the primary chemical composition cellulose) as the carbon precursor and silicon sol as the SiO_2 source for the synthesis of SiC nanowires and nanopatricles by carbothermal reduction in static argon atmosphere, and the carbothermal conversion of the carbon–silica composites was investigated by TG, IR, XRD, SEM, and TEM techniques.

Experimental procedure

Sample preparation

Silica sol was prepared from ethanol solutions of tetraethoxysilane [$Si(OC_2H_5)_4$, TEOS], distilled water and

W. Wang (✉) · Z. H. Jin · T. Xue · G. B. Yang · G. J. Qiao
State Key Laboratory for Mechanical Behavior of Materials, Xi'an Jiaotong University, Xian 710049, P.R. China
e-mail: wangwei9310023@mail.xjtu.edu.cn

ammonia at a suitable molar ratio of TEOS:H_2O:NH_3 by a Sol–Gel process as that described elsewhere [20]. In the present work, the concentration of silica sol was equal to 20% by weight. Filter paper (Hang Zhou Filter paper Co. Ltd) was used as a carbon precursor. A silica sol was added to a segment of filter, the amount of sol added was controlled until the filter paper/silica sol weight ratio was 2:1 when dried at 100 °C overnight in air. The dried filter paper/silica sol composite was placed in alumina boat and carbonized in a horizontal tube furnace at desired temperatures (about 800 °C) for one hour with a heating rates of 2°C/min. The whole treatment was preformed in N_2 atmosphere, and carbon/silica composites were formed in the end of carbonization.

Carbothermal reduction of the as-prepared carbon/silica composites was carried out in static argon atmosphere in a graphite heater furnace at 1550 °C with a rate of 600 °C /h to form SiC nanomaterials. The reactant carbon/silica composites loaded in graphite crucibles were placed into the hot zone of the furnace. The temperature of the furnace was raised up to the designed temperature, and then held for 1 h to allow completions of reactions between silica and carbon to form β-SiC. The flow chart for the whole preparation process is shown in Fig. 1.

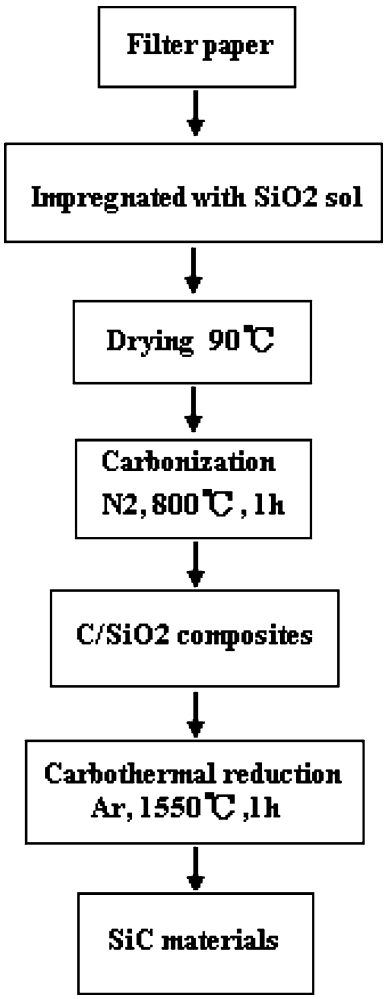

Fig. 1 Processing scheme of manufacturing SiC nanomaterials

Characterization

The carbonized behavior of filter paper was characterized using thermogravimetric analysis (TG) in a N_2 flow-rate of 40 mL/min with a heating rate of 10 °C/min from room temperature to 800 °C. TG was performed on Netzsch STA 409C thermal analyzer.

The morphological changes of the starting material during the transformation of filter paper/silica and carbon/silica composites into SiC nanomaterials were observed and analyzed by scanning electron microscopy (SEM, Hitachi, S-2700) operated at 20 kV and 20 mA. The microstructure of the produce was observed by transmission electron microscope (TEM). X-ray diffraction (XRD) was measured on a D/MAX-RA X-ray diffractometer to determine the crystalline phases formed during the carbothermal reduction reaction. Infrared spectroscopy (IR) studies were performed with a infrared spectrometer (AVATAR 360 FT-IR, Nicolet) in the wavenumber range of 4000–400 cm^{-1}.

Results and discussion

TG curve of filter paper

Figure 2 shows the TG curve of filter paper up to 850 °C. It can be seen that weight loss in N_2 atmosphere starts below 100 °C and almost terminates at 600 °C. The maximum in decomposition rates of filter paper is in the temperature range 260–340 °C, and corresponding weight loss is 36%.

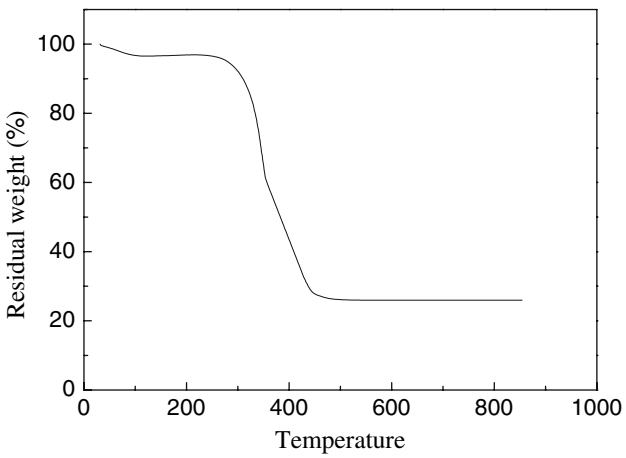

Fig. 2 Thermogravimetric curves of filter paper

A second weight loss of 35% occurs between 340 and 520 °C. The residual carbon mass is 25%.

The primary chemical composition of filter paper is cellulose. Mechanisms [21] involved in conversion of cellulose to carbon are: (a) desorption of adsorbed water up to 150 °C, (b) splitting off of cellulose structure water between 150 and 240 °C, (c) chain scissions, or depolymerization, and breaking of C–O and C–C bonds within ring units evolving water, CO and CO_2 between 240 and 400 °C, (d) aromatization forming graphitic layers above 400 °C, and (e) completion of the decompositions and rearrangements, leaving a carbon template structure. Cellulose break down in a stepwise manner at 260–520 °C, and almost 75% of the total weight loss occurs due to evolution of H_2O, CO_2, and volatile hydrocarbon species from fragmentation reactions of the polyaromatic components.

XRD analysis of resulting SiC materials

Figure 3 shows the XRD patterns of carbon (Fig. 3a, carbonized from filter paper), carbon/silica composite (Fig. 3b) and resulting SiC materials (Fig. 3c). The two broad peaks centered around 22° and 44° in Fig. 3a, b suggest that carbon and carbon/silica composite are amorphous. The previous study showed that the crystallinity of the resulting carbon from the thermal decomposition of filter paper increased to a more graphitic-like microstructure with the increase of carbonization temperature [22], even though they were non-graphitizable carbon [23]. Peaks due to β-SiC (cubic type) phases in Fig. 3c are observed together with the broad peaks due to carbon, indicating that the formation of β-SiC has taken place and the residual free carbon still exists. There exist four main strong peaks at $2\theta = 35.71°$, 41.46°, 60.06° and 71.84°, which are attributed, respectively, to the (111), (200), (220) and (311) planes of the cubic type (β-SiC) phase. In addition, one peak at lower diffraction angle than of the strong (111) peak stack, which is result from the stacking faults similar to those of previously reported [24, 25].

FTIR analysis

Figure 4 shows the FTIR spectra of the formed carbon/silica composite and resulting SiC materials prepared from carbon/silica composites. In the IR spectrum (Figure 4a) of the carbon/silica composite, the absorption bands at 1090, 800 and 466 cm^{-1} are attributed to antisymmetric and symmetric stretching vibrations of Si–O–Si bond, respectively. Compared with the spectrum in Fig. 4a, the abovedmentioned absorption bands nearly disappear in Fig. 4b. At the same time, a new intense broad band centred at 825 cm^{-1} is observed, which is ascribed to the Si–C fundamental stretching vibration, showing that the carbothermal reduction is almost completed.

SEM analysis

Figure 5 show typical SEM images of carbon/silica composite (Fig. 5a) and the synthesized SiC materials (Fig. 5b). It is seen that the carbon originated from cellulose fiber was covered by SiO_2 gel particles, shown disorderly arrangement without any direction. The SEM micrographs of the resulting SiC material shown there are nanowires and nanoparticles. The materials are composed of SiC nanowires with the maximal lengths of up to 10 μm,

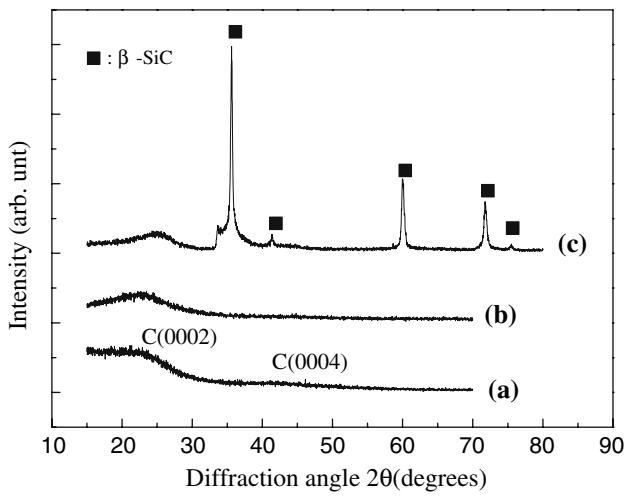

Fig. 3 Powder XRD patterns of (**a**) carbon carbonized from filter paper (**b**) carbon/silica composite and (**c**) SiC prepared from carbon/silica composites

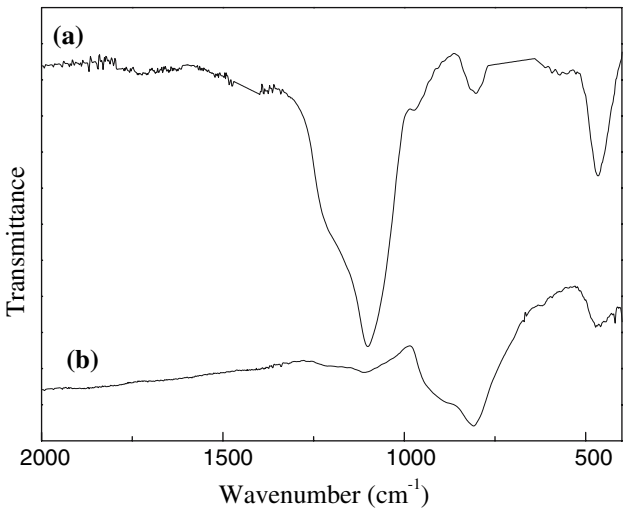

Fig. 4 Infrared spectra of (**a**) carbon/silica composite and (**b**) SiC prepared from carbon/silica composites

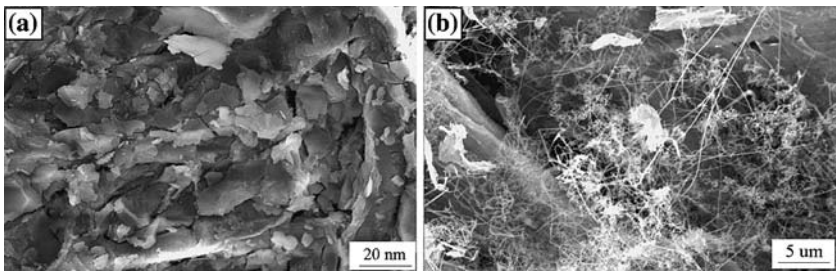

Fig. 5 SEM micrographs of (**a**) carbon/silica composite and (**b**) SiC nanowires prepared from carbon/silica composites

and some particles with typical diameter of about 2 μm can be observed in Fig. 5b. The SiC nanowires possess diameters of 50–200 nm, their length is in the range from hundreds of nanometers to several micrometers. At the same time, there are lots of particles, which are the result of the reaction between gaseous SiO and solid carbon. In the literature [26], half of the initial carbon is supposed to be released from template via CO (g) evaporation leaving a higher porosity in the resulting SiC materials. From the observations it is concluded that the SiC formed is highly porous in the initial state of reaction, making rapid gas transport possible. Therefore, the SiC nanowires generate spontaneously through the reaction between gaseous SiO and gaseous carbon monoxide CO.

TEM analysis

Figure 6 shows the TEM images and SAED pattern of the sample. It can be seen that crystalline SiC nanoparticles have average size between 40 and 100nm, and the corresponding SAED pattern is shown in Fig. 6(d), the three strong polycrystalline rings in accordance with cubic SiC [(111), (220) and (311)] confirm the XRD result. Besides the nanoparticles, some nanowires and nanorods are also observed (Fig. 6(a)), it can be seen that the average diameter of SiC nanowires is in the 20–200 nm range and the length is over several ten microns. The selected-area electron diffraction patterns from the nanowires in Fig. 6(b) can be indexed to the cubic β-SiC structure. The yield of SiC nanomaterials to the total product is about 50%.

Mechanism of conversion of carbon/silica composite into SiC nanowires

The overall carbothermal reduction between carbon and silica for producing silicon carbide can be described as depicted in Eq. 1.

$$SiO_2\ (s, l) + 3C\ (s) \rightarrow\ SiC\ (s) + 2CO\ (g) \qquad (1)$$

In fact, reaction (1) proceeds through two stages in which a gaseous intermediate, silicon monoxide (SiO) gas is generated. The first step consists of a solid–solid or

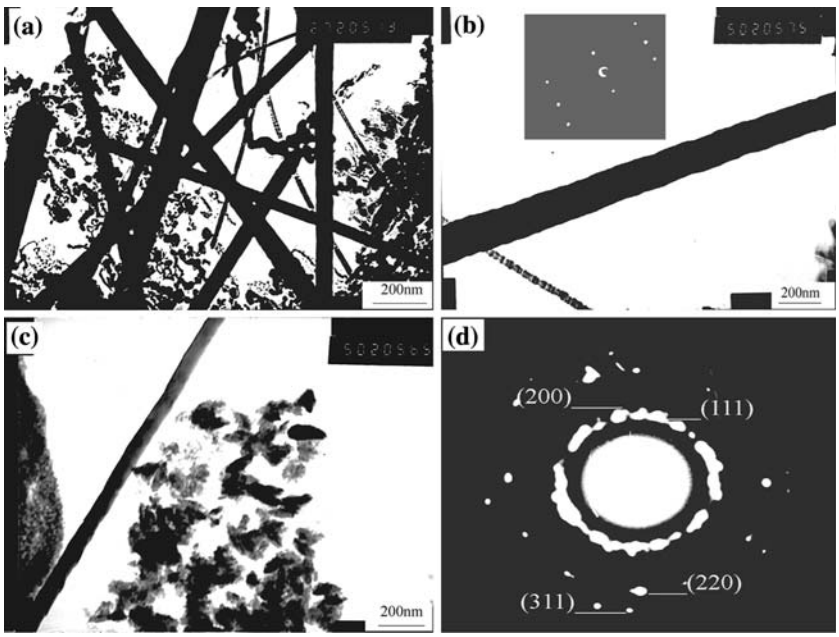

Fig. 6 (**a**) TEM micrographs of SiC nanowires and nanoparticles. (**b**) TEM and SAED images of SiC nanowires. (**c**) TEM images of SiC nanoparticles. (**d**) SAED pattern of SiC nanoparticles

solid–liquid type of reaction between carbon and silica leading to the formation of gaseous silicon monoxide (SiO) and carbon monoxide (CO) according to reaction (2),

$$SiO_2\ (s, l) + C\ (s) \rightarrow SiO\ (g) + CO\ (g) \quad (2)$$

where s, l and g in the brackets refer to solid, liquid and gas state respectively. Once carbon monoxide (CO) is formed, SiO maybe produced according to reaction

$$SiO_2\ (s) + CO\ (g) \rightarrow SiO\ (g) + CO_2\ (g) \quad (3)$$

Since a significant amount of carbon remains in the material, any CO_2 produced will be consumed immediately by the Boudouard reaction (4) to form CO gas.

$$CO_2\ (g) + C\ (s) \rightarrow\ 2CO\ (g) \quad (4)$$

In these reactions, carbon is either a CO_2 getter or a CO generator, which keeps the CO_2/CO ratio low enough to make the reduction of SiO_2 possible by gas phase CO.

In a second step, the gaseous SiO subsequently reacts further with carbon according to the following gas-solid reaction:

$$SiO\ (g) + 2C\ (s) \rightarrow SiC\ (S) + CO\ (g) \quad (5)$$

The SiO vapor from Eqs. 2 and 3 reacts with carbon to yield SiC (s) nuclei heterogeneously on the surfaces of carbon through Eq. 5, which is a commonly accepted mechanism of SiC formation [27, 28]. In general, as soon as SiC forms on carbon, the growth process via Eq. 5 can be hindered by either the solid diffusion of carbon or the diffusion of SiO gas molecules through SiC layer. The formation of SiC nanowires can not be explained by the gas–solid reaction of SiO(g) and C (S). It is more likely that the nanowires formed via gas–gas reaction between SiO(g) and CO(g). The reaction can express as follow:

$$SiO\ (g) + 3CO\ (g) \rightarrow SiC\ (S) + 2CO_2(g) \quad (6)$$

Reaction (6) favors the growth of SiC nanowires that are similar to those obtained by chemical vapor deposition with SiO and CO as the primary reactants in the literature [29].

Thermodynamic analysis of reactions

The carbothermal reduction of SiO_2 is controlled by atmosphere, pressure, temperature and time. The total reaction (1) is strongly endothermic with $\Delta H^{298} = 618.5$ kJ mol^{-1} and performs in two steps. The initial reaction (2) is also endothermic whereas the second reaction (5) is exothermic.

The temperature, at which the reaction is initiated, is strongly dependent on pressure and atmosphere composition. A high pressure will shift the start of the reaction (2) to higher temperatures as it is shown for the pressure dependence in Fig. 7(a), which is derived from $\Delta G = \Delta G^o + \Delta nRT \ln(p/p^o)$ with $\Delta G^o = G_{SiO} + G_{CO} - G_{SiO2}$. The data of G are obtained from Reference [30] ($\Delta n = 2$ for reaction (2), R = gas constant, T = temperature). One can also reach this shift to higher temperatures by a high carbon monoxide partial pressure. When reaction (2) is inhibited the SiO content is rather low and reaction (5) will be also inhibited, in this situation no SiC is formed over the whole temperature range where $\Delta G > 0$ kJ mol^{-1}, consequently no silicon carbide exists up to 1800 °C at a pressure >180 kPa and no silicon carbide crystals with growth and coarsen in this period. If the pressure is rapidly decreased at a temperature of more than 1550 °C the reaction (2) and (5) start extremely vigorously.

For the reactions path 2–6, their free energy changes with temperature and pressure of system are shown in Figs. 7a–e, respectively. As far as chemical equilibrium is concerned, the smaller the value of ΔG, the larger is the equilibrium constant K, and the more the products when equilibrium state is attained. Therefore, the reaction 3 ($\Delta G > 0$) can not process in the temperature range 1100–2100 k. From Fig. 7c, it is found that the free energy change of reaction 4 is negative in the whole temperature range, which indicate that reaction 4 is a spontaneous reaction in the condition. The reaction 5 is different with others reactions as $\Delta n = 0$, the pressure can not effect on chemical equilibrium, moreover, the influence of temperature to free energy change is so small that it can be neglect. The reaction 6 favors the growth of SiC nanowires and nanoparticles that are formed via gas-gas reaction, the lower temperature and the bigger pressure, and the process of this reaction is easier.

From the thermodynamic data of reaction 2–6 in the temperature range 1100–2100 k, SiC nanowires were formed through the different reaction steps. The SiO vapor form Eq (2) reacts with carbon to yield SiC nuclei heterogeneously on the surfaces of carbon through Eq. 5. As soon as SiC formed, the growth process via Eq. 5 could be hindered by either the solid diffusion of carbon or the diffusion of SiO gas molecules through SiC, the continuing growth of SiC(s), therefore, could result only through Eq. 6 to form SiC nanowires by a vapor reaction between SiO and CO [27]. The growth mechanism of SiC nanowires may be explained by the vapor–solid (VS) process, with some degree of similarity to that proposed by Lewis [31].

The total mixture of silica and carbon is converted in a short period under these conditions especially when they are intrinsic mixed in a colloidal level, which will shorten the diffusion paths so that the reaction kinetics need not

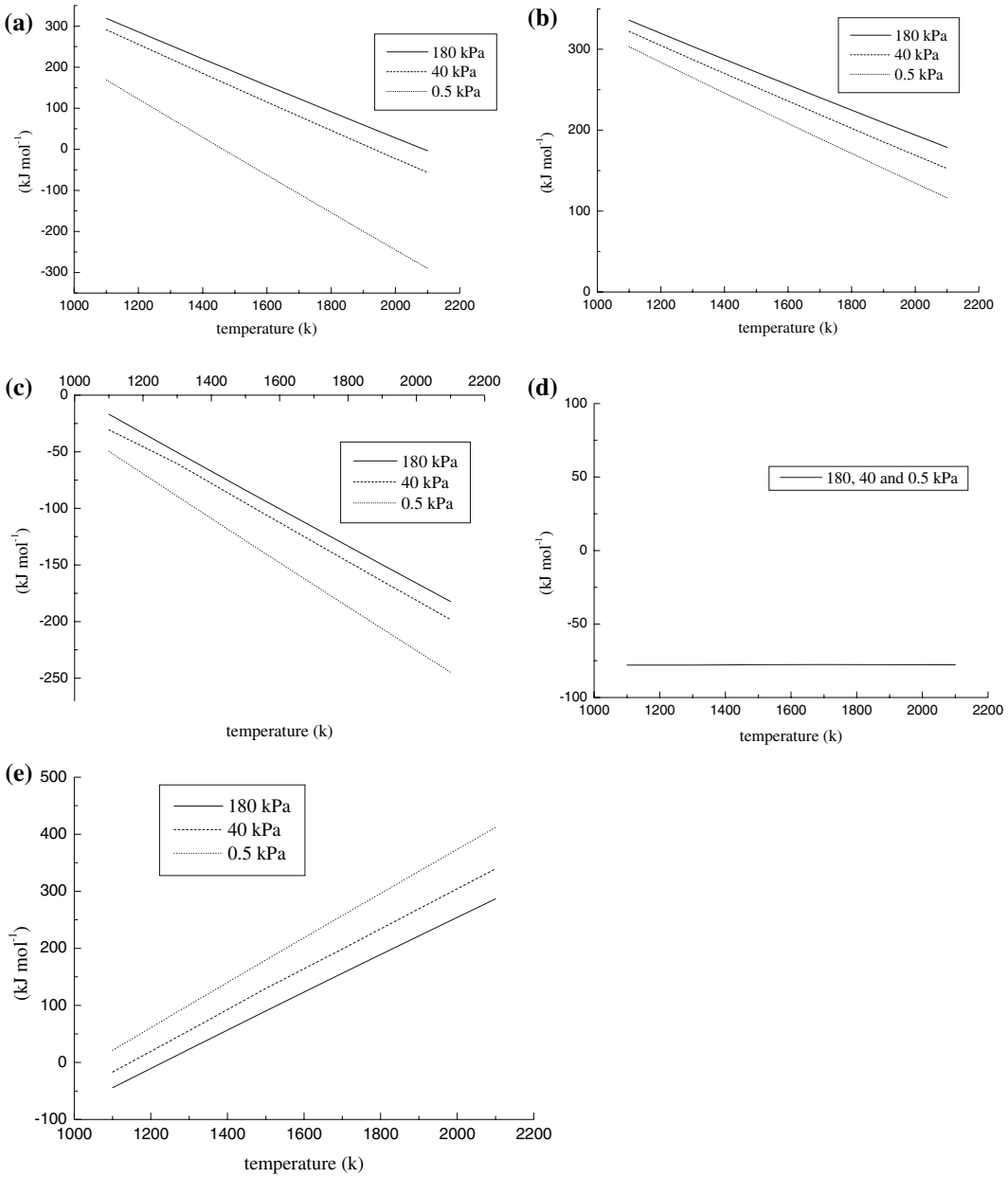

Fig. 7 Change of free energy ΔG for reaction 2(a), 3(b), 4(c), 5(d) and 6(e) depending on temperature and pressure

consideration. This principle was applied in our investigations and the results were discussed in this paper.

Conclusions

SiC nanowires and SiC nanoparticles were prepared at 1550 °C for 1 h in a static argon atmosphere by sol–gel and carbothermal reduction techniques using TEOS and filter paper as the starting materials. XRD indicate that the final SiC materials is composed of β-SiC, and the residual free carbon still exists. SEM and TEM reveal that SiC nanowires is single crystal wires with diameters ranging from 50 to 200 nm and their lengths over several tens of microns. SiC nanowires are formed by gas-gas reaction of SiO (g) and CO (g), and attributed to vapor-solid (VS) growth mechanism.

Acknowledgement The authors gratefully acknowledgement the financial supports from the National Natural Science Foundation of China (No. 50572084).

References

1. Dai HJ, Wong EW, Lu YZ, Fan SS, Lieber CM (1995) Nature 375:769
2. Yang PD, Lieber CM (1996) Science 273:1836

3. Xiia Y, Yang P, Sun Y, Wu Y, Mayers B, Gates B, Yin Y, Kim F, Yan H (2003) Adv Mater 15:353
4. Wong EW, Sheehan PE, Lieber CM (1997) Science 277:1971
5. Wu ZS, Deng SZ, Chen J, Zhou J (2002) Appl Phys Lett 80:3829
6. Zhang HF, Wang CM, Wang SL (2002) Nano Lett 2:941
7. Wu X, Song W, Huang W, Pu M, Zhao B, Sun Y, Du J (2001) Mater Res Bull 36:847
8. Meng G, Zang L, Qin Y, Feng S, Mo C, Li H, Zhang S (1999) J Mater Sci Lett 18:1255
9. Liang C, Meng G, Zhang L, Wu Y, Cui Z (2000) Chem Phy Lett 329:323
10. Shi W, Zheng Y, Peng H, Wang N, Lee CS, Lee ST (2000) J Am Ceram Soc 83:3228
11. Morales AM, Lieber CM (1998) Science 279:208
12. Yu DP, Lee CS, Bello I, Sun XS, Tang YH, Zhou GW, Bai ZG, Zhang Z, Feng SQ (1998) Solid state commun 105:403
13. Sharma NK, Williams WS (1984) J Am Ceram Soc 67:715
14. Kajiwara M (1986) J Mater Sci 21:2254
15. Seo W-S, Koumoto K (2000) J Am Ceram Soc. 83(10):2584–2592
16. Zhang LD, Meng GW, Phillipp F (2000) Mater Sci Eng A 286:34–38
17. Meng GW, Cui Z, Zhang LD, Phillipp F (2000) J Cry Grow 209:801–806
18. Shin Y, Li XH, Wang CM et al (2004) Adv Mater 16(14):1212–1215
19. Streitwieser DA, Popovska N, Gerhard H, Emig G (2005) J Eur Ceram Soc 25:817–828
20. Qian JM, Wang JP, Qiao GJ, Jin ZH (2004) J Eur Ceram Soc 24:3251–3259
21. Greil P (2001) J Eur Ceram Soc 21(2):105–118
22. Greil P, Lifka T, Kaindl A (1998) J Eur Ceram Soc 18:1975–1983
23. Cheng HM, Endo H, Okabe T, Saito K, Zheng GB (1999) J Porous Mater 6:233–237
24. Koumoto K, Takeda S, Pai CH, Sato T, Yanagida H (1989) J Am Ceram Soc 72(10):1985–1987
25. Liang CH, Meng GW, Zhang LD, Wu YC, Cui Z (2000) Chem Phys Lett 329:323–328
26. Paccaud O, Derre A (2000) Chem Vapor Depos 6(1):33–40
27. Guterl CV, Ehrburger P (1997) Carbon 35(10–11):1587–1592
28. Martin HP, Ecke R, Muller E (1998) J Eur Ceram Soc 18(12):1737–1742
29. Saito M, Nagashima S, Kato A (1992) J Mat Sci Lett 11(7): 373–376
30. Barin J (1989) Thermochemical data of pure substances, Vols. 1 and 2. VCH, Weinheim
31. Lewis B (1974) J Cryst Growth 21:29